



Mutant Hoxd13 induces extra digits in a mouse model of synpolydactyly directly and by decreasing retinoic acid synthesis

Pia Kuss,^{1,2,3} Pablo Villavicencio-Lorini,^{1,2} Florian Witte,^{1,2,3} Joachim Klose,⁴ Andrea N. Albrecht,¹ Petra Seemann,¹ Jochen Hecht,⁵ and Stefan Mundlos^{1,2,5}

¹Max Planck Institute for Molecular Genetics, Berlin, Germany. ²Institut für Medizinische Genetik, Charité, Universitätsmedizin Berlin, Berlin, Germany. ³Institut für Chemie-Biochemie, Freie Universität Berlin, Berlin, Germany. ⁴Institut für Humangenetik, Charité, Universitätsmedizin Berlin, Berlin, Germany. ⁵Berlin-Brandenburg Center for Regenerative Therapies, Charité, Universitätsmedizin Berlin, Berlin, Germany.

Individuals with the birth defect synpolydactyly (SPD) have 1 or more digit duplicated and 2 or more digits fused together. One form of SPD is caused by polyalanine expansions in homeobox d13 (*Hoxd13*). Here we have used the naturally occurring mouse mutant that has the same mutation, the SPD homolog (*Spdh*) allele, and a similar phenotype, to investigate the molecular pathogenesis of SPD. A transgenic approach and crossing experiments showed that the *Spdh* allele is a combination of loss and gain of function. Here we identify retinaldehyde dehydrogenase 2 (*Raldh2*), the rate-limiting enzyme for retinoic acid (RA) synthesis in the limb, as a direct *Hoxd13* target and show decreased RA production in limbs from *Spdh/Spdh* mice. Intrauterine treatment with RA restored pentadactyly in *Spdh/Spdh* mice. We further show that RA and WT *Hoxd13* suppress chondrogenesis in mesenchymal progenitor cells, whereas *Hoxd13* encoded by *Spdh* promotes cartilage formation in primary cells isolated from *Spdh/Spdh* limbs, and that this was associated with increased expression of *Sox6/9*. Increased *Sox9* expression and ectopic cartilage formation in the interdigital mesenchyme of limbs from *Spdh/Spdh* mice suggest uncontrolled differentiation of these cells into the chondrocytic lineage. Thus, we propose that mutated *Hoxd13* causes polydactyly in SPD by inducing extraneous interdigital chondrogenesis, both directly and indirectly, via a reduction in RA levels.

Introduction

Limb malformations are a relatively common human birth defect. From a clinical point of view, they can be subdivided into brachydactylies (short digits), reduction defects, and duplications, the latter affecting most frequently the digits, in which case they are called *polydactyly* (1, 2). Polydactylies may occur at the anterior side (thumb, preaxial), the posterior side (little finger, postaxial), or between fingers (central). Early transplantation experiments have shown that a complete duplication of the autopod can be induced by implanting an additional zone of polarizing activity (ZPA) to the anterior (opposite) region of the limb bud. In this case, the bud receives 2 signals, one from the posterior side and an additional one from the anterior side, resulting in an autopod with mirror image duplication. The signaling molecule sonic hedgehog (Shh) was identified as the major signal from the ZPA that is necessary and sufficient to confer these effects (reviewed in refs. 3–5).

Misregulation of Shh signaling and misexpression of Shh at the anterior region of the limb bud was shown to be a major factor in the pathogenesis of polydactyly (3, 6). For example, mutations in the so called ZPA regulatory sequence (ZRS) of Shh result in ectopic expression of Shh at the anterior limb bud, thus inducing polydactyly (7–9). Mutations in *Gli3*, one of the transcriptional effectors of Shh signaling, result in polydactyly in mice and humans by

disturbing the balance between the activator and the suppressor function of *Gli3* (10). Dysfunction of the cilia can lead to polydactyly, for example in Bardet-Biedl, oral-facial-digital, Senior-Loken, and Meckel-Gruber syndromes, probably reflecting a role for cilia in hedgehog signaling (11), as studies in polydactylous mouse mutants with abnormal intraflagellar transport proteins were shown to have defective *Gli3* processing (12). Genes such as *Alx4* interfere with Shh signaling and produce polydactyly also by inducing Shh misexpression (13). Curiously, misregulation of another member of the hedgehog family, Indian hedgehog (*Ihh*), results in polydactyly in doublefoot mice through expression of *Ihh* in the anterior limb margin (14).

Duplications of digits are frequently associated with cutaneous or osseous webbing of the adjacent fingers, resulting in syndactyly, hence the name *synpolydactyly* (SPD) for these conditions (15). One type of SPD has been shown to be caused by mutations in homeobox d13 (*Hoxd13*), the most 5' homeobox (*Hox*) gene of the D cluster. *Hox* genes of the A and D clusters are expressed in a graded overlapping fashion throughout the posterior limb. Through this specific pattern, positional cues are thought to be conferred to the cells (16). For example, in the absence of *Hoxa13* and *Hoxd13*, the autopods fail to develop (17) and removal of *Hoxa11* and *Hoxd11* function leads to truncations of the zeugopod (18), whereas a deficiency of groups 9 and 10 affects the stylopod (19). While these results point to an important role for *Hox* genes in early patterning of the limb, an additional role in the subsequent process of skeletal organogenesis and growth is likely (20).

Interestingly, the mutations associated with SPD have been shown to be expansions of an Ala repeat located within the N-terminal part of the protein. These mutations result in an expansion

Conflict of interest: The authors have declared that no conflict of interest exists.

Nonstandard abbreviations used: chMM, chicken micromass; *Hox*, homeobox; *Hoxd13*, homeobox d13; RA, retinoic acid; *Raldh2*, retinaldehyde dehydrogenase 2; Shh, sonic hedgehog; SPD, synpolydactyly; *Spdh*, SPD homolog.

Citation for this article: *J. Clin. Invest.* 119:146–156 (2009). doi:10.1172/JCI36851.

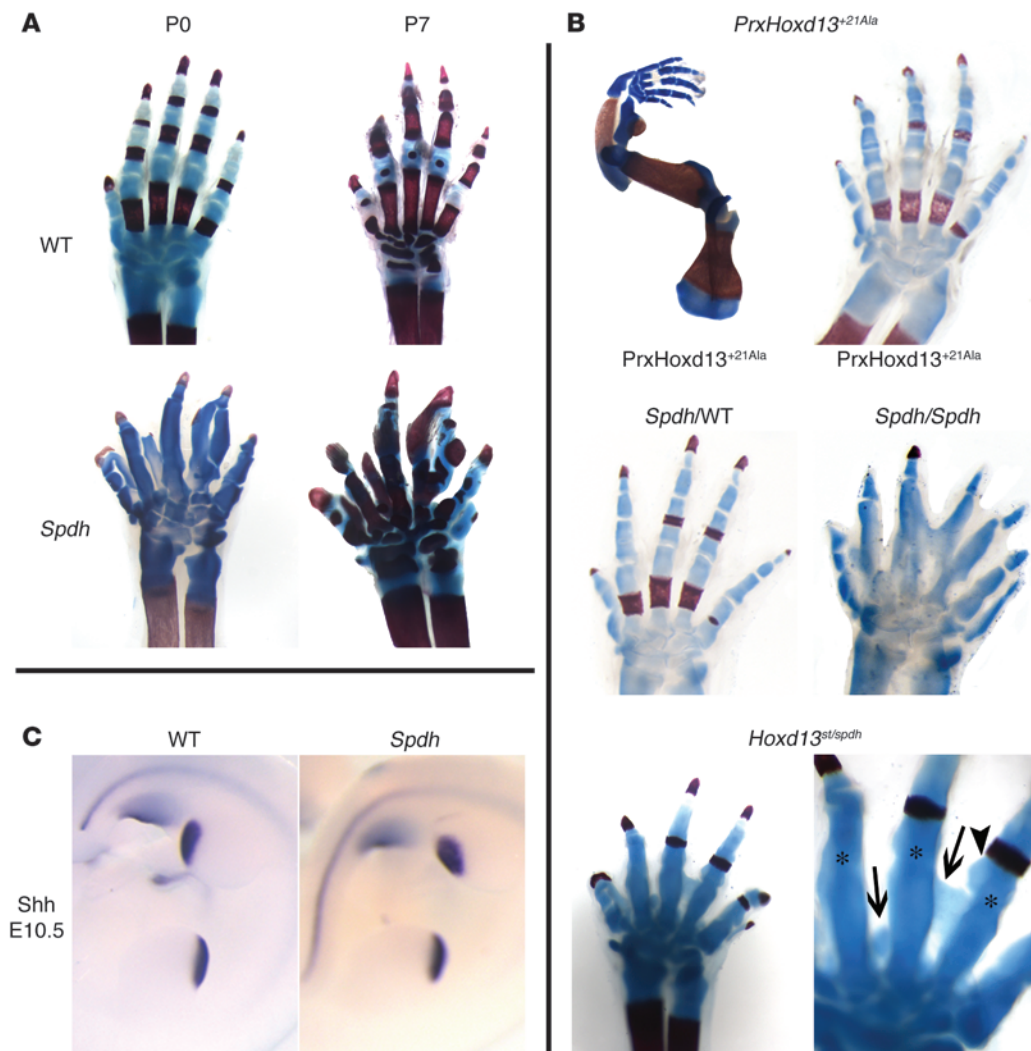


Figure 1

The *Spdh* allele acts as a loss and gain of function. (A) Skeletal preparations of WT and *Spdh/Spdh* mice at birth (P0) and 1 week of age (P7). *Spdh/Spdh* mice exhibited multiple additional incompletely formed digits, fused joints, and a severe delay in ossification. Cartilage was stained with Alcian blue, bone with Alizarin red. (B) Skeletal preparations of transgenic *PrxHoxd13^{+21Ala}* mice at P0 showed a severe malformation of the radius and bending of the ulna. No major changes were seen in the digits. Introducing 1 *Spdh* allele (*Hoxd13^{+21Ala}; Spdh/WT*) did not change the phenotype. Mice expressing *Hoxd13^{+21Ala}* on a homozygous *Spdh* background (*Hoxd13^{+21Ala}; Spdh/Spdh*) showed a severe phenotype with excessive fusions and polydactyly. Mice with 1 *Spdh* allele and 1 inactivated *Hoxd13* allele (*Hoxd13^{st/spdh}*) showed a delay in bone formation, fusion of joints, occasional postaxial polydactyly, and a short digit 2. In addition, ectopic cartilage formation between the digits, and an uneven surface of the digit cartilage (magnification of interdigital space shown on right), was present. Original magnification, $\times 3.2$ (left), $\times 4.0$ (right). (C) *Shh* expression in E10.5 WT and *Spdh* embryos.

of a 15-Ala repeat by an additional 7 to 14 Ala (21, 22). The specificity of these mutations was underlined by the identification of a mouse mutant with an identical mutation and a similar phenotype, which was consequently termed *SPD homolog (Spdh)* (23), and the lack of similar changes in *Hoxd13* knockout mice (17). Similar mutations were subsequently described in a number of other genes. All mutations affect transcription factors and result in expansions with a total length of more than 21 Ala (24). For some of these mutations, a loss-of-function mechanism is likely, as similar phenotypes occur in association with (for example) nonsense mutations in the same gene. For *Hoxd13*, however, the mechanism appears to be different, as shown by breeding experi-

ments of *Spdh* mice with various Hox mutants (25). The expansion of the Ala repeat in *Hoxd13* results in degradation of the mutant protein in the proteasome. Insufficient degradation leads to the accumulation of aggregates within the cell. These effects correlate with the length of the repeat, i.e., the longer the repeat, the more protein is degraded and the more aggregates are present. This mechanism appears to apply for all polyalanine repeat expansions and can thus be considered as the pathomechanism behind the disease (26). In spite of these advances in understanding the pathology of polyalanine-related conditions, it remains unclear why the mutations in *Hoxd13* result in SPD and how the dominant mechanism can be explained.

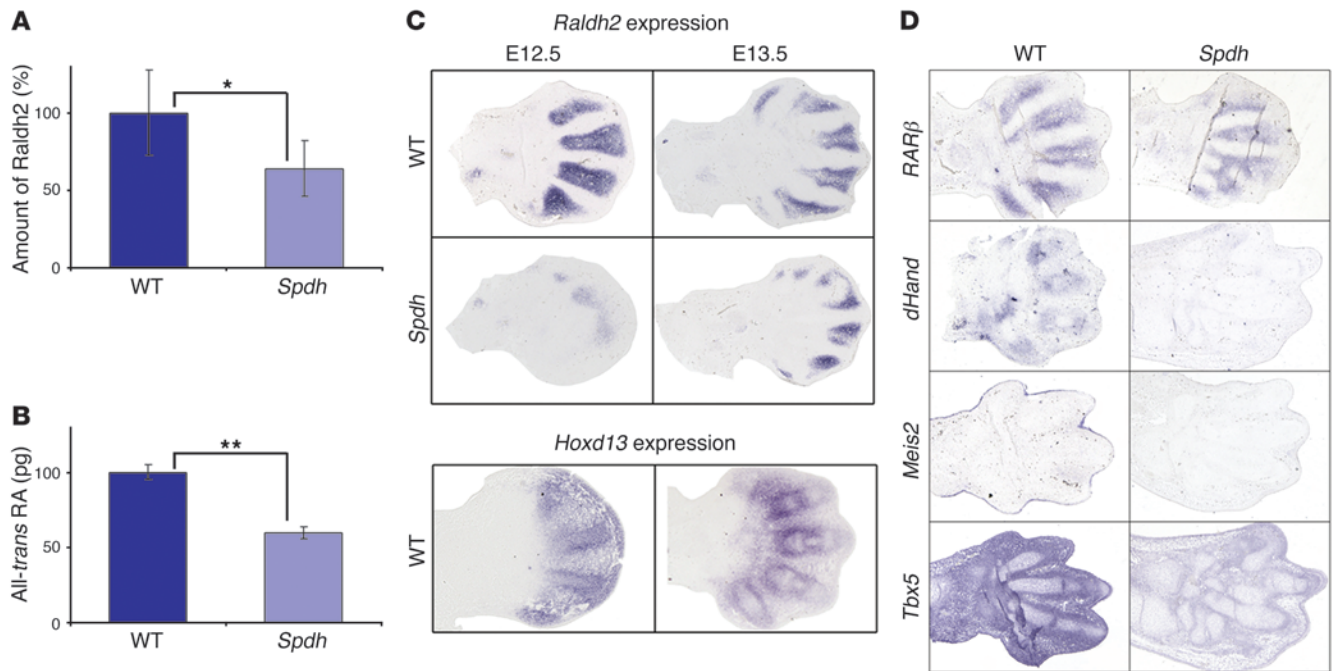


Figure 2

Dysregulation of RA pathway in *Spdh*. (A) 2D gel electrophoresis of limb bud tissue (stage E13.5) demonstrated a reduction (63% of WT) of Raldh2 protein levels in *Spdh* mice ($*P < 0.05$). (B) Quantification of RA in E13.5 autopod limb tissue. *Spdh* limbs show a reduction to 57% when compared to WT ($**P \leq 0.005$). (C) In situ hybridization against *Raldh2* on forelimbs at E12.5 and E13.5 demonstrated a reduction of *Raldh2* mRNA in *Spdh* limbs. In the WT limbs, *Raldh2* was expressed in the interdigital space but not the cartilaginous condensations. At E13.5, Raldh2 expression was mainly found in the perichondrium. Expression overlapped with *Hoxd13*. (D) In situ hybridizations of WT and *Spdh* forelimbs at E13.5 of RA downstream targets *RARβ*, *dHand*, *Meis2*, and *Tbx5*. All showed reduced expression in *Spdh* limbs.

Using screening approaches we identify the retinoic acid-producing (RA-producing) enzyme retinaldehyde dehydrogenase 2 (*Raldh2*) as downregulated in *Spdh* limb buds. We show that *Hoxd13* regulates *Raldh2* and that RA represses chondrogenesis in the interdigital space, preventing the formation of cartilage condensations. In the *Spdh* mutant, less *Raldh2* results in lower RA levels in the limb and thus less inhibition of chondrogenesis. In addition, we show that WT *Hoxd13* is a strong repressor of chondrogenesis, whereas *Hoxd13* with expanded Ala repeats has a pro-chondrogenic effect, contributing to the accelerated and uncontrolled differentiation of interdigital cells into chondrocytes. We propose that *Hoxd13*-associated polydactyly in *Spdh* mice is due to increased chondrogenesis in the interdigital mesenchyme.

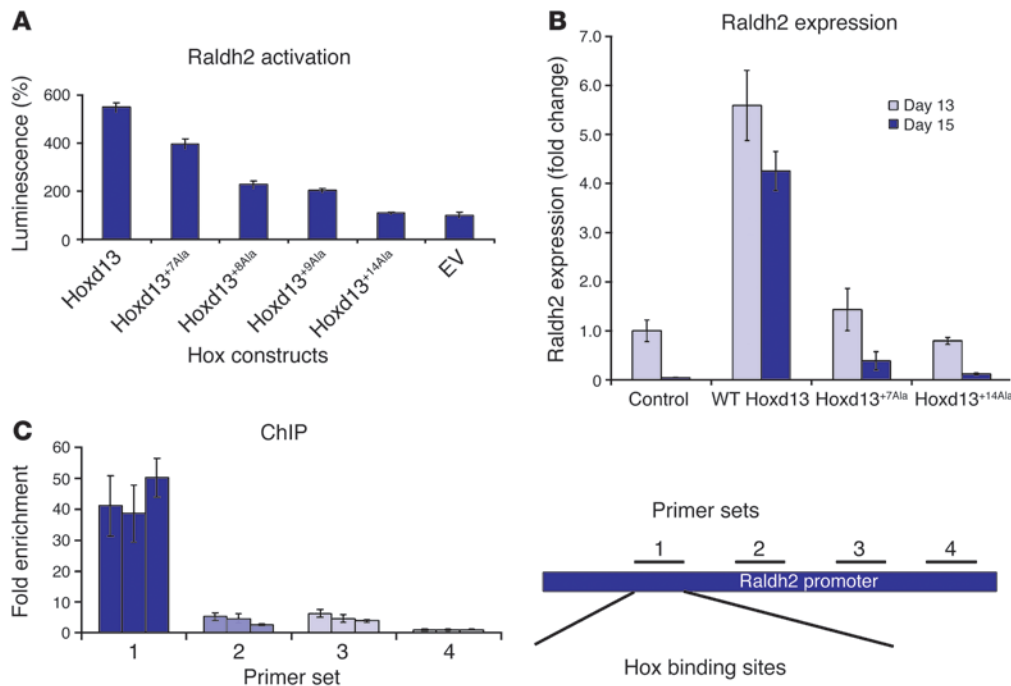
Results

Spdh is a combination of partial loss of function and gain of function. Figure 1A shows representative skeletal preparations stained with Alcian blue (cartilage) and Alizarin red (bone) of WT and *Spdh/Spdh* forelimbs at postnatal days P0 and P7. *Spdh/Spdh* mice exhibited additional digits at varying locations, fused joints, and a severe delay in ossification. To test whether polyalanine expansions result in a dominant phenotype we expressed a *Hoxd13* mutant containing a +21 Ala expansion under the control of the limb-specific *Prx1* promoter (*PrxHoxd13^{+21Ala}* mice). Two mouse lines were obtained, both showing the same phenotype: bowing of the ulna and, apart from a delay in ossification, normal digits (Figure 1B). This phenotype did not change significantly after introducing 1 *Spdh* allele. These results indicate that even a very long polyalanine is not sufficient

to induce polydactyly on a WT or heterozygous *Spdh* background. However, crossing *PrxHoxd13^{+21Ala}* mice on a homozygous *Spdh* background resulted in a much more severe phenotype than that found in single *Spdh/Spdh* mice. To further investigate interactions of mutant *Hoxd13* with other *Hoxd* genes, we crossed *Spdh/+* mice with mice in which 1 allele of *Hoxd13* was inactivated (*Hoxd13^{st/st}*) (27). Double heterozygous (*Hoxd13^{st/Spdh}*) mice showed an intermediate phenotype overlapping with, but also distinct from, the single homozygous (*Spdh/Spdh, Hoxd13^{st/st}*) mice. Similar to our observations of *Spdh/Spdh* mice, we observed severe abnormalities of joint formation and a delay in ossification. However, central polydactyly did not occur. Instead, postaxial polydactyly was occasionally present, similar to what has been described in *Hoxd13^{st/st}* mice (27). Close examination of the interdigital space, however, revealed ectopic cartilage formation between the digits and irregular boundaries of the digital cartilage. Neither abnormality is present in *Hoxd13^{st/st}* mice (27) but were part of the *Spdh/Spdh* phenotype (Figure 1B).

Polydactyly frequently involves *Shh* misexpression, and *Shh* was shown to regulate Hox expression (28). We thus investigated *Shh* expression in WT and *Spdh* limbs at various stages without observing significant differences in distribution or intensity of *Shh* mRNA (Figure 1C).

Raldh2 is downregulated in *Spdh* limbs. To identify pathways that were misregulated in *Spdh* limbs, we used a dual approach and screened for differences in protein and mRNA expression levels between WT and mutant limbs. We observed downregulation of genes known to be part of the RA signaling pathway (data not shown), including *Raldh2*. In addition, we performed 2D gel electrophoresis to screen

**Figure 3**

Regulation of *Raldh2* by *Hoxd13*. **(A)** Luciferase reporter assay of a conserved region of murine *Raldh2*. Cos7 cells were transfected with *Raldh2* reporter and *Hoxd13* expression constructs carrying different Ala repeat length mutations (+7, +8, +9, +14). WT *Hoxd13* activated *Raldh2*. Increasing length of the Ala repeat results in loss of activation. Error bars show SEM. EV, empty vector. **(B)** Quantitative PCR of chMM cultures showed upregulation of *Raldh2* by WT *Hoxd13*. Infections with *Hoxd13*^{+7Ala} and *Hoxd13*^{+14Ala} were comparable with uninfected controls. Error bars show SD. **(C)** ChIP confirmed binding of WT *Hoxd13* to the *Raldh2* promoter. ChIP from chMM cultures was done with 4 different primer pairs. Real-time PCR with primer set 1 showed an approximately 45-fold enrichment of the *Raldh2* promoter fragment precipitated with *Hoxd13*. Sets of 3 bars represent results from 3 independent experiments. Error bars show SD.

for changes at the protein level, and *Raldh2* was identified as being downregulated (63% of WT levels) (Figure 2A). Since *Raldh2* converts retinol into RA (29), we measured RA content in E13.5 limb buds. This quantification revealed a reduction of all-*trans* RA in *Spdh/Spdh* limbs to 57% of WT values (Figure 2B).

To investigate the *Raldh2* expression pattern and level, we performed in situ hybridization on serial sections of limb buds at different developmental stages (Figure 2C). At E12.5, we observed a distinct expression pattern of *Raldh2* within the interdigital space between the condensations. With further development (E13.5), *Raldh2* continued to be expressed in the interdigital mesenchyme, but the strongest expression was present in the perichondrium. In the mutant *Raldh2*, expression was almost absent at E12.5 and strongly reduced at E13.5. No expression was observed in the perichondrium. *Raldh2* and *Hoxd13* showed overlapping expression patterns in the mouse autopod at E12.5 and E13.5 (Figure 2C).

To further test our hypothesis of altered RA signaling, we performed expression analysis of different established RA signaling targets (Figure 2D). In our studies, *RARβ* was expressed more weakly in *Spdh/Spdh* than in WT forelimbs, and expression in the perichondrium was not observed at all. *dHand*, normally expressed in the digital chondrogenic regions, was downregulated. Likewise, *Meis2* expression was reduced in *Spdh/Spdh* mutants. In WT mice, *Tbx5* was expressed ubiquitously all over the limb bud (Figure 2D). In *Spdh/Spdh* mutant limbs, we observed a downregulation of *Tbx5* expression.

forms were comparable with uninfected controls. Direct binding of *Hoxd13* to the endogenous *Raldh2* promoter was shown by ChIP. Using 4 primer pairs covering different regions containing putative Hox binding sites of the *Raldh2* promoter, we found the product of primer pair 1 (–4,900 to –4,849 bp relative to the transcription start site) to be enriched 38- to 50-fold compared with primer pair 4 (–1,169 to –1,115 bp relative to the transcription start site) (Figure 3C). Primer pairs 2 and 3 were only enriched 2.5- to 6-fold.

RA suppresses chondrogenesis. To investigate of the influence of RA on primary cells with a potential to differentiate, we used the chMM system. In this model system, mesenchymal limb bud cells are seeded at high density, inducing spontaneous differentiation into various cell lineages, including cartilage. The degree of cartilage formation was measured by staining with Alcian blue and subsequent quantification using AxioVision Outmess software (Figure 4A). Cultures were treated with increasing doses of RA or, alternatively, with increasing doses of the following 2 inhibitors of RA synthesis: disulfiram, known to block *Raldh* (30), and citral, which blocks both steps of vitamin A oxidation (31). Our experiments demonstrate an antichondrogenic dose-dependent effect of RA on mesenchymal cells. Disulfiram and citral enhanced chondrogenesis in chMM cultures, indicating that RA negatively regulates chondrogenic differentiation in limb mesenchymal cells.

To test the effect of RA on chondrogenesis in vivo, we implanted RA-soaked beads in chicken limb buds, harvested those 24 hours

Raldh2 is regulated by *Hoxd13*. To test whether *Raldh2* is directly regulated by *Hoxd13*, we performed different promoter assays. In silico analysis revealed a conserved region 3,300 bp upstream from the transcription start site of murine *Raldh2*. Within a 1,300-bp region, several Hox binding sites were identified that were conserved between *Homo sapiens* and rat. This region was cloned into pGL2, and enhancer and luciferase reporter assays were performed in Cos7 cells transfected with *Raldh2* reporter and different *Hoxd13* constructs. WT *Hoxd13* activated the *Raldh2* promoter (Figure 3A). Mutated *Hoxd13* showed a reduction in activation depending on the length of the repeat. To test a possible regulation in cells naturally expressing *Hoxd* genes, quantitative PCRs were performed on chicken micro-mass (chMM) cultures after infection with RCAS virus carrying the WT or mutant *Hoxd13* (Figure 3B). *Hoxd13* was shown to upregulate *Raldh2*, whereas the mutated

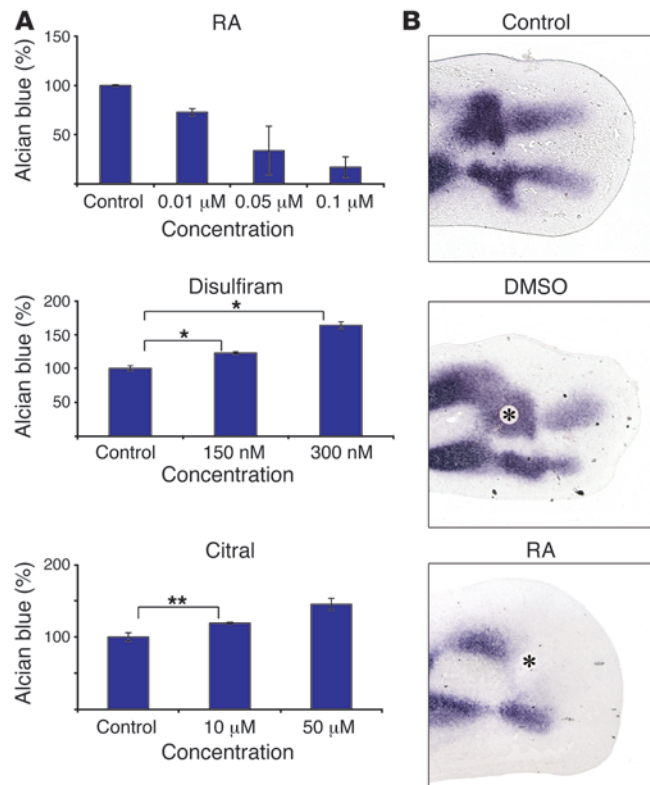


Figure 4

RA inhibits chondrogenesis. (A) ChMM cultures were treated with various concentrations of RA or RA inhibitors (disulfiram, citral), cultured, stained with Alcian blue, and quantified. Intensity of staining in controls is 100%. Note the reduction of chondrogenesis after RA treatment and induction after treatment with RA antagonists. Results are presented as mean \pm SD. * P < 0.05; ** P < 0.005. (B) Bead implantations in chicken limb buds at Hamburger Hamilton (HH) 27 with subsequent *Col2a1* section in situ hybridization after 20 hours of incubation. Top: Control without bead. Middle: DMSO-soaked control bead with unchanged *Col2a1* expression. Bottom: Limb after implantation of RA-soaked beads. Note the suppression of *Col2a1* expression. Asterisks indicate beads.

amounts of Alcian blue-positive matrix. To test whether this effect could be inhibited by blocking RA, we treated infected cells with disulfiram. We observed a moderate increase in chondrogenesis (data not shown), indicating that other pathways in addition to RA are important for Hoxd13-induced suppression of chondrogenesis in this system. To test the effect of mutant Hoxd13 on chondrogenesis, we performed the same experiments expressing Hoxd13 with an expanded polyalanine repeat (+7 Ala and +14 Ala). At day 9, induction of chondrogenesis was comparable with controls, indicating a loss of inhibition. Thereafter, the mutant showed an increase in cartilage formation when compared with the control. This effect became apparent at day 11 and was most pronounced on days 13 and 15. Using quantitative PCR we analyzed the expression of *Col2a1*, the predominant collagen of cartilage (Figure 6B). We observed an almost complete suppression of *Col2a1* in cells with WT Hoxd13 expression throughout the tested period. The 2 mutant forms, i.e., Hoxd13^{+7Ala} and Hoxd13^{+14Ala}, showed no suppression of *Col2a1* expression on day 9 and, as expected from the results obtained with Alcian blue staining, increased *Col2a1* expression at day 13. To test whether other Hox genes had a similar effect, we expressed Hoxd11, Hoxd12, and Hoxa13 in chMM cultures and measured Alcian blue incorporation (Figure 6C). Hoxd11 and Hoxd12 had no major effect on cartilage formation, indicating that the observed antichondrogenic effect was specific for Hoxd13. In contrast, Hoxa13, similar to Hoxd13, is also a strong suppressor of chondrogenesis.

Enhanced chondrogenesis and polydactyly formation in Spdh/Spdh limbs.

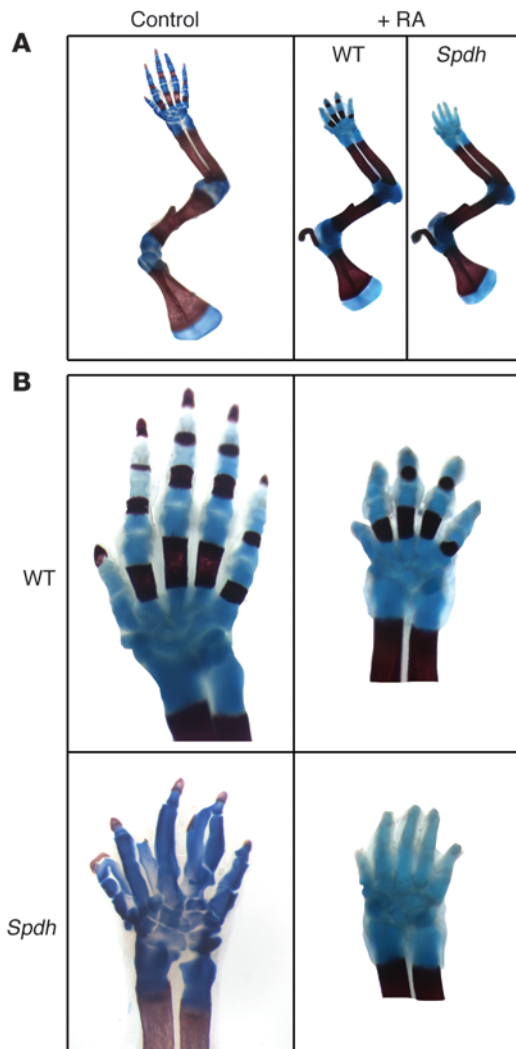
To further investigate the chondrogenic potential of mesenchymal cells in *Spdh/Spdh* autopods, we isolated cells at E13.5, the stage at which the mutant limbs can be visibly distinguished from WT, and cultured them at high density. Chondrogenesis was determined at days 3, 6, and 9 by staining with Alcian blue and image quantification. Cells from *Spdh/Spdh* autopods showed a much stronger potential to form cartilaginous nodules compared with cells from control animals, indicating that the Hoxd13 mutation has a pro-chondrogenic effect (Figure 7A).

To further investigate the chondrogenic potential of interdigital mesenchyme in *Spdh/Spdh* limbs, we analyzed mutant limbs at E12.5, the stage at which the first cartilage condensation forms that will later develop into the digits. At these stages chondrogenesis has to be repressed in the interdigital mesenchyme and promoted at the sites where the digits form. In WT mice this results in restricted expression of *Sox9* (Figure 7B), the gene that is pivotal for cartilage formation (32, 33), to the cartilaginous condensations. In contrast, *Spdh/Spdh* mice showed *Sox9*-positive cells dispersed throughout the interdigital mesenchyme (Figure 7B). Furthermore, the border between positive and negative cells is blurred, both at E12.5 and

later, and performed section in situ hybridization with a *Col2a1*-specific probe to detect cartilage using collagen type II expression as a marker. The results showed that RA treatment results in a complete inhibition of chondrogenesis in the digits (Figure 4B).

Intrauterine treatment of Spdh mice with RA rescues the polydactyly phenotype. Our results indicated that dysregulation of RA signaling plays a role in the *Spdh* phenotype. To verify this hypothesis, we aimed at adjusting the level of RA by intrauterine supplementation. Pregnant females were treated with orally administered 5 μ g RA/g body weight once per day from E8.5 to E14.5. Newborn animals were analyzed by skeletal preparation, and WT littermates served as controls (Figure 5). RA, a known teratogene, led to a reduction in size of the entire limb both in WT and in *Spdh/Spdh* animals (Figure 5A). All mutant offspring showed exactly 5 digits instead of the usual 6 or 7 condensations (Figure 5B). For statistics, 30 offspring animals were analyzed, including 8 WT, 8 mutant, and 14 heterozygous animals, fitting to the expected ratio. The size reduction was similar between the animals, and the observed effects were reproducible and stable.

Hox genes modulate chondrogenesis. To test the influence of Hoxd13 on chondrogenesis, we expressed WT and mutant *Hoxd13* in chMM culture using the NCI RCAS retroviral system. This system resulted in a moderate expression of the target gene in close to 100% of cells. Western blot analysis (data not shown) demonstrated that the expression levels were moderate and that mutant Hoxd13 was partially degraded, as previously shown (26). Expression of WT *Hoxd13* had a profound effect on cartilage formation, as evidenced by the almost complete suppression of chondrogenesis (Figure 6A). Control chMM cultures began to form cartilaginous nodules on day 6, followed by a continuous increase of Alcian blue-positive tissue. In contrast, cells treated with WT Hoxd13 produced minute

**Figure 5**

RA treatment rescues the polydactyly phenotype. **(A)** Newborn animals were analyzed with skeletal preparations. WT littermates served as controls. Bone was stained in red, cartilage in blue. RA led to an overall reduction in bone size both in WT and *Spdh* compared with an untreated control. Size reduction was comparable in WT and *Spdh/Spdh* mice. **(B)** Comparison of the autopod of untreated controls (left) with RA-treated animals (right) demonstrated an overall reduction in size but normal formation of digits, cartilage, and bone in WT animals. Treated *Spdh/Spdh* offspring had 5 digits, demonstrating a partial rescue of the *Spdh* phenotype.

administration of RA to anterior chicken limb buds results in anterior-posterior duplications (35). RA signaling appears to be important for at least 2 different time points during development (36). In the early phase, RA is essential for the initiation of limb budding from the lateral plate mesoderm. Later, the main role of RA appears to be as a proximodistal signal during apical ectodermal ridge formation and in the induction of *Shh* expression (37). The latter function partly depends on RA-mediated induction of *Hox* genes, which in turn activate *Shh* (38). However, in spite of these known functions of RA, its definite role in limb development remains controversial. Active RA is produced by retinaldehyde dehydrogenases (*Raldh1–3*), enzymes that catalyze the second oxidative step in the biosynthesis of RA from retinol (29). *Raldh2* is responsible for most of the RA-synthesizing activity and for initiating RA signaling during early mouse embryogenesis, as shown in *Raldh2*^{-/-} embryos that have severe midline defects and do not form limb buds at all (36, 37). Due to the severe phenotype, late effects of *Raldh2* deficiency were not investigated. We show that *Raldh2* is expressed at E12.5 and E13.5 when the digital anlagen are formed. The expression is confined to the interdigital mesenchyme and the perichondrium, thus overlapping with *Hoxd13* expression at these stages. Our results show that *Raldh2* expression in the interdigital mesenchyme is reduced in *Spdh/Spdh* mice. Furthermore, the expression at the margins of the condensations (perichondrium) is completely missing in mutant mice, and residual activity is restricted to the most distal regions of the developing limb.

The deficiency of *Raldh2* in *Spdh* mice suggests the possibility of direct regulation of *Raldh2* by *Hoxd13*. Direct promoter and ChIP analysis and the upregulation of *Raldh2* in chMM that expressed *Hoxd13* suggest a direct regulation of *Raldh2* by *Hoxd13*. Reduced amounts of *Raldh2* should result in reduced RA concentrations. This was verified by direct RA measurement in limb tissue demonstrating a reduction by approximately 40% in *Spdh/Spdh* limbs. Our hypothesis of reduced RA signaling is additionally supported by the downregulation of several known RA targets including the RA receptor *RARβ*, *Tbx5*, *Meis2*, and *dHand* (36, 39–41).

Besides its role in early patterning, RA signaling was shown to play a role in the regulation of chondrogenesis. Earlier studies have shown that RA is able to inhibit chondrogenesis *in vitro* (42). This effect was shown to be most pronounced in cells derived from the more proximal limb bud indicating that the late blastemal stage of chondrogenesis is most vulnerable to RA treatment (43). *In vivo*, low doses are reported to enhance chondrogenesis, whereas high doses result in inhibition of cartilage formation (44, 45). Loss of RA receptor-mediated signaling was shown to be necessary and sufficient for expression of the chondroblast phenotype (46). Part of this effect is likely to be transmitted via *Sox9*, a transcription factor required for cartilage formation (47, 48). Furthermore, RA signaling antago-

E13.5. These findings are consistent with our *in situ* hybridization data, which show expression of *Sox9* mRNA (Figure 7C) at the same sites. Quantitative PCR of chMM cultures revealed that mutant *Hoxd13* activated *Sox9* and *Sox6* expression (Figure 7D).

To document the nature and time point of the additional condensations, 3D models of developing limbs were generated (Figure 7E). Serial paraffin-embedded sections of E12.5 and E14.5 were hybridized with a *Col2a1* probe to visualize cartilaginous condensations, photographed, and reconstituted with Amira software. In contrast to the WT limbs, *Spdh/Spdh* limbs showed multiple additional condensations in the proximal parts of the interdigital region. Some of these condensations developed in the interdigital mesenchyme independent of regular digit condensations, while others were connected to future digits. Thus, we concluded that cartilage formation in *Spdh* mutants does not represent a true digit formation but rather an uncontrolled process of enhanced differentiation at multiple sites.

Discussion

Our results indicate that RA signaling is disturbed in *Spdh* mice. RA was initially identified as a crucial signaling factor in limb bud development based on the observations that exogenous RA produces duplications in regenerating axolotl limbs (34). Furthermore,

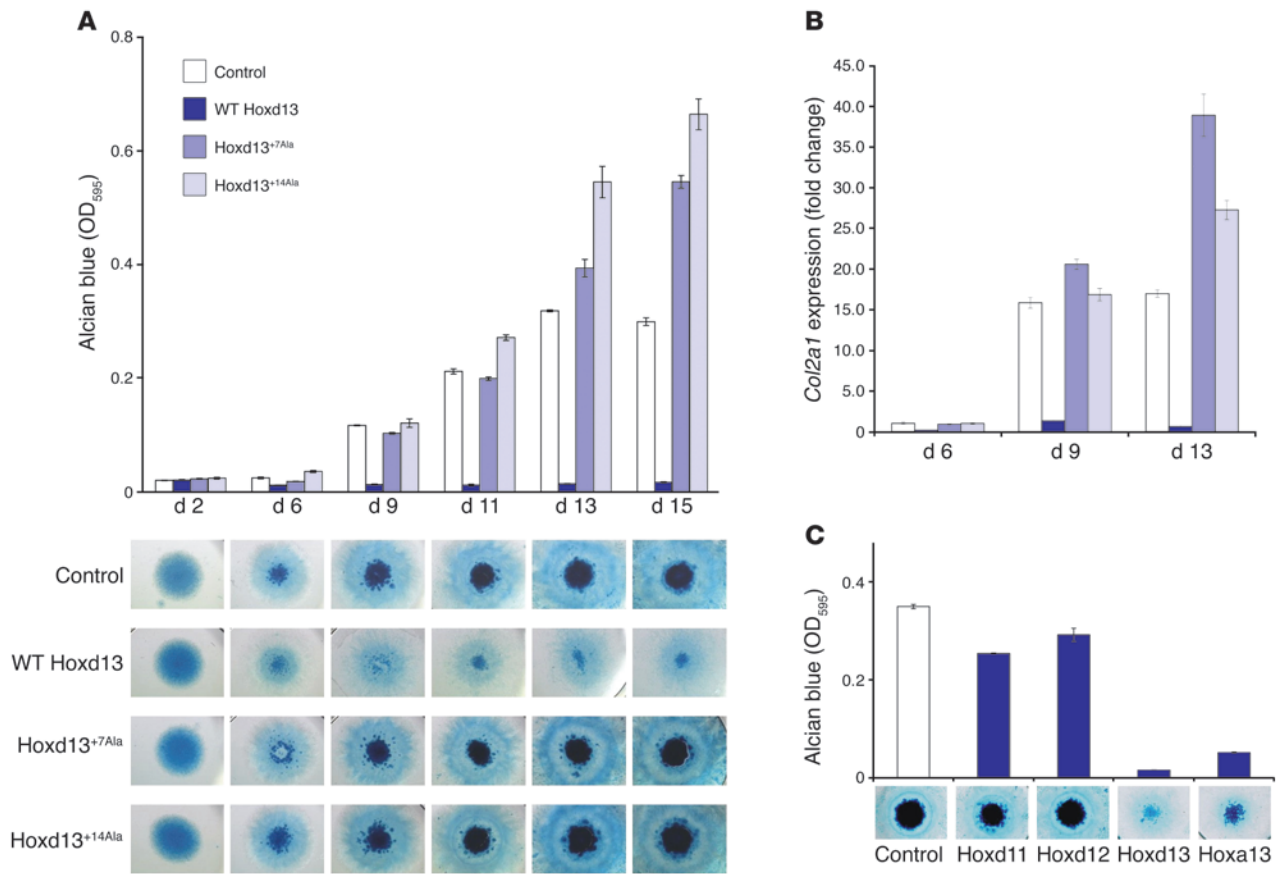


Figure 6

Hoxd13 modulates chondrogenesis. (A) WT and mutant Hoxd13 were expressed in chMM cultures using the NCI RCAS retroviral system. Alcian blue staining was used to detect cartilage-specific nodules starting at day 6 (bottom) and subsequently quantified (top). WT Hoxd13 inhibited cartilage formation, while mutant Hoxd13 with +7Ala or +14Ala expansions had a prochondrogenic effect. (B) Quantitative PCR analysis of chMM cultures. Values were normalized to day 6 control. WT Hoxd13 strongly suppressed *Col2a1* expression, while Hoxd13 with expanded Ala repeats showed increased expression. (C) The effects of other autopod-expressed Hox genes were analyzed in chMM cultures. Hoxd11 and Hoxd12 showed only a mild inhibitory effect on chondrogenesis. In contrast, Hoxa13 had an effect similar to Hoxd13. Results are presented as mean ± SD.

nizes the prochondrogenic effects of bone morphogenetic proteins (BMPs), and BMP4 downregulates *Raldh2* expression, thus influencing RA levels (46). Our experiments in chMM cultures confirm these results and show that RA suppresses chondrogenesis, whereas RA antagonists enhance cartilage formation. Thus, RA appears to be an important factor in the organogenesis of the skeleton by negatively influencing the differentiation of mesenchymal cells into chondrocytes. This antichondrogenic effect is reduced in *Spdh/Spdh* mice due to lower levels of RA in the interdigital mesenchyme.

Our results indicated that RA levels in *Spdh/Spdh* mice are moderately downregulated. This may explain the lack of more severe phenotypes such as limb truncations. On the other hand, the timing of *Raldh2* regulation by Hoxd13 in the phase of skeletal organogenesis is likely to be a key factor in the determination of the phenotype. The limb phenotype of *Raldh2*^{-/-} mice can be partially rescued by oral administration of RA to pregnant females (37). We thus treated pregnant *Spdh* mice with low doses of RA via intragastric feeding to test whether the phenotype can be rescued. Our results show that the polydactyly phenotype of *Spdh/Spdh* mice can be rescued, indicating that RA deficiency indeed plays a significant role in the pathogenesis of *Spdh*-related polydactyly.

In previous studies it was described that RA depletion results in premature and ectopic expression of Hox genes in early limb buds (37). Activation of Hox gene transcription by RA response elements and RA has previously been documented, and RA has been shown to trigger collinear activation of Hox genes in cells (49, 50). RA is known to play a role in the sequential activation of Hox genes in limb development by promoting anterior Hox genes and delaying posterior ones (51). The expression of Hox genes has been extensively studied in *Spdh* mice (25, 52). No differences were identified, indicating that the level of RA dysregulation in *Spdh* mice is not sufficient to induce misexpression.

Polyalanine expansions as they occur in *Spdh* mice are unlikely to be pure loss-of-function mutations, as inactivation of Hoxd13 alone does not result in a SPD phenotype. However, inactivation of the most posterior Hoxd genes together (Hoxd11, -d12, and -d13) results in SPD, similar to that observed in *Spdh* mice, but less severe (53). This indicates that the mutant Hoxd13 acts in a dominant-negative manner, possibly by negatively interacting with other Hox genes (25). To investigate this hypothesis further, we created the *PrxHoxd13^{+21Ala}* transgenic mouse line. These mice showed a major deformity of the radius and the ulna but only minor changes in their autopods. Thus,

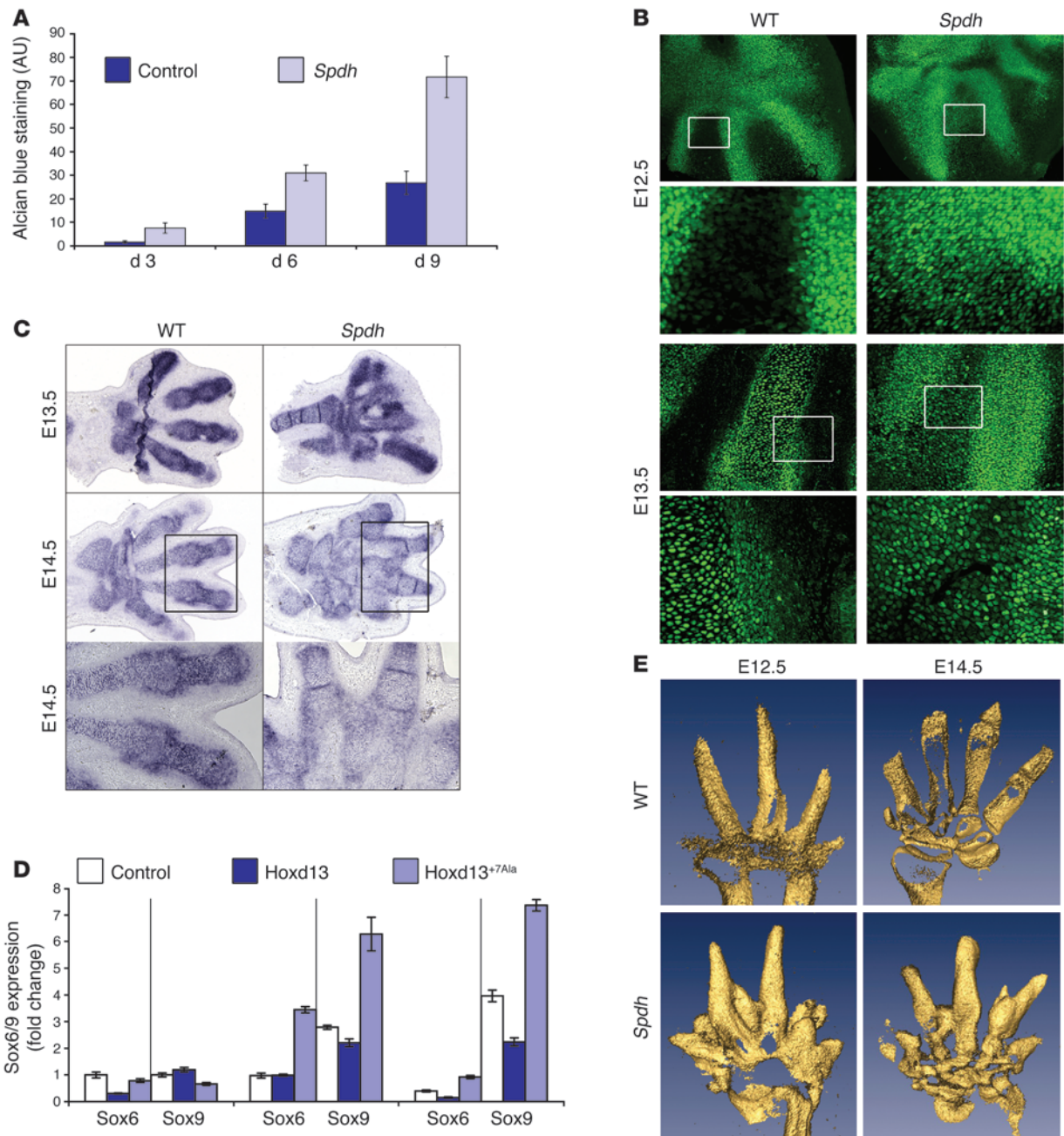


Figure 7

Enhanced chondrogenesis in *Spdh/Spdh* limbs. **(A)** Primary mesenchymal cells of E13.5 *Spdh/Spdh* autopods grown in vitro at high density, stained for Alcian blue, and quantified. Note the increased chondrogenesis in mutant limbs. Results are presented as mean ± SEM. **(B)** Immunohistochemistry with anti-Sox9 antibody on E12.5 and E13.5 limb sections. WT showed Sox9 in the cartilaginous anlagen but not in the interdigital mesenchyme. In *Spdh* limbs, no exact border could be determined, and cells within the interdigital mesenchyme were Sox9 positive. Boxed areas show magnification. Original magnification (from top to bottom), ×100, ×400, ×200, ×400. **(C)** In situ hybridization for Sox9 at stages E13.5 and E14.5 demonstrated expression in the interdigital mesenchyme of *Spdh* limbs. **(D)** Regulation of Sox6 and Sox9 in chMM cultures at days 6, 9, and 13 (left to right). RNA was extracted from chMM cultures, and transcribed cDNA was measured by quantitative PCR. Values were normalized to day 6 control. Mutant *Hoxd13* activated Sox6/9 expression. Results are presented as mean ± SD. **(E)** 3D models of WT and *Spdh/Spdh* limbs stained for *Col2a1* expression after in situ hybridization. Note additional condensations within interdigital spaces in *Spdh* limbs (arrows).

based on the alterations in the stylopod, *Hoxd13*^{+21Ala} is not a complete loss of function but is insufficient to induce a distal limb phenotype on a WT *Hoxd13* background. Even if 1 WT allele is replaced by a *Spdh* allele (*PrxHoxd13*^{+21Ala}; *Spdh*/WT), no major effect was observed.

On a homozygous *Spdh* background (*PrxHoxd13*^{+21Ala}; *Spdh/Spdh*), however, we observed a very severe phenotype. This indicated that 1 WT *Hoxd13* allele was sufficient to prevent the effect of even a very long Ala expansion mutant. Crossing *Spdh* mice with mice carrying 1



inactivated *Hoxd13* allele resulted in a distinct phenotype consisting of features described for *Hoxd13* inactivation, such as shortening of digit 2 and postaxial polydactyly (27), as well as features of the *Spdh* spectrum, including abnormal joints, irregularities of the cartilaginous digits, and a delay in ossification. In addition, we observed ectopic cartilage between the digits, sometimes bridging the digits, which we interpreted as a minimal *Spdh* phenotype. Thus, *Spdh* is likely to result in a loss of *Hoxd13* function together with a residual gain of function. The latter is different from WT *Hoxd13* and can thus be called neomorphic. This effect is dosage dependent and occurs only in the absence of a WT *Hox* allele.

In order to investigate the proposed neomorphic effect further, we expressed WT and mutant *Hoxd13* in chMM cultures using the NCI RCAS retroviral system. Our experiments demonstrate that WT *Hoxd13* and *Hoxa13* are strong suppressors of chondrogenesis. In contrast to WT, mutant *Hoxd13* with an expanded Ala repeat induces chondrogenesis. To investigate the reason of the observed effect, we quantified the expression of *Sox9* and *Sox6*, 2 transcription factors known to be essential and sufficient to induce chondrogenesis. Our results indicated that mutant *Hox* directly or indirectly activates *Sox6/9* genes, which in turn promotes chondrogenesis. This effect was also observed *in vivo*. Whereas WT limbs showed a very restricted *Sox9* expression pattern strictly confined to the cartilaginous condensations, *Spdh* limbs showed aberrant expression of *Sox9* in cells of the interdigital mesenchyme. The enhanced chondrogenic potential of cells expressing mutant *Hoxd13* was also demonstrated in *Spdh/Spdh* derived mesenchymal limb cells, a finding that further substantiates our hypothesis.

We conclude that at least 2 mechanisms contribute to the *Spdh* phenotype that are likely to function in an combined manner. In WT, RA suppresses chondrogenesis in the interdigital mesenchyme. In *Spdh/Spdh* mice carrying a mutant *Hoxd13* with expanded Ala repeats, *Raldh2* is downregulated, resulting in less RA and, consequently, increased cell differentiation. This hypothesis is further supported by the phenotype of RA receptor compound knockouts that also present with additional interdigital cartilage anlagen (54). *Hoxd13*, which is expressed in the interdigital mesenchyme, functions as a repressor of chondrogenesis and cell differentiation. Mutants with Ala expansions lose this repressive activity. Instead, they show a neomorphic effect by inducing chondrogenesis. The combination of loss of suppression and gain of induction results in aberrant condensations in the interdigital mesenchyme and thus polydactyly. In contrast to other polydactylies such as those involving the *Shh* pathway, these condensations do not develop into true digits, but rather represent an uncontrolled process of enhanced differentiation at multiple sites. This is somewhat similar to the ectopic formation of cartilage anlagen with subsequent polydactyly observed after apical ectodermal ridge or ectoderm removal (55). Hence, we propose a pathomechanism for *Hoxd13*-related SPD, which is not the result of a defect in patterning, but rather of irregularities in differentiation.

Methods

Mice. *Spdh* mice were obtained from The Jackson Laboratory (23). Mutant offspring were generated by breeding *Spdh*/WT females to *Spdh*/WT males. Timed matings were produced, and 12 pm on the day of vaginal plug was considered E0.5. DNA from tail tip, amnion, or liver was used for genotyping, which was performed as described previously (52).

Transgenic *Hoxd13* mice carrying *Hoxd13* with additional 21 Ala under the control of *Prx* promoter (*PrxHoxd13*^{21Ala} mice) were created by DNA injection into oocytes. Two stable lines carrying the transgene were

obtained. Two PCR reactions specific for the *Prx* promoter construct and Ala repeat length served for genotyping. Skeletal preparations were performed as previously described (52).

All-trans RA (Sigma-Aldrich; catalog R2625) was suspended in 100% EtOH (50 mg/ml), diluted in sunflower oil to the required dose, and administered orally (5 µg/g body weight) to pregnant *Spdh*/+ females once a day from E8.5 to E14.5. RA was cooled on ice and protected from light during handling. Newborn litters were analyzed with skeletal preparations (described above), and WT littermates served as controls. All animal experiments were approved by the Landesamt für Gesundheit und Soziales (Berlin, Germany).

RNA extraction and quantification. To minimize effects of random biological variation, limbs from different litters were frozen in liquid nitrogen and then pooled after genotyping (30 WT or *Spdh/Spdh* forelimbs for each hybridization). RNA was extracted with peqGold Trifast (peqLab Biotechnologie GmbH) according to the manufacturer's instructions. Extraction was followed by DNase treatment (RNase-Free DNase Set; Qiagen), purified with RNeasy Mini-Kit (Qiagen), and analyzed by Affymetrix GeneChip analysis.

2D electrophoresis. Tissue of 40 WT and *Spdh* limb buds each were collected at E13.5, and frozen in liquid nitrogen until genotyping was done. 2D gel electrophoresis was performed as previously described (56). Protein spots were identified with MALDI-TOF analysis, and differences in protein amount were scaled by volume.

RA measurement. For RA measurement directly out of limb tissue limb buds of stage E13.5 were collected. Preparation was done in red light darkness; limbs were directly frozen in liquid nitrogen and stored at -80°C. After genotyping, 6 limbs were pooled per sample. Measurement was done by As Vitas, and 3 independent experiments were performed.

In situ hybridization. For *in situ* hybridization, limbs were fixed in 4% PFA, dehydrated, and embedded in paraffin. Sections (5 µm) from different E12.5, E13.5, E14.5, and E16.5 were hybridized with specific probes. To avoid cross-hybridization, probes were generated from 3' UTR with 2 specific primers each. *Raldh2*, forward, ATGGGTGAGTTTGCTTACG, reverse, CCTGCTGGAAGGACTCAAAG; *RARβ*, forward, AGCAAGCCTCACATGTTTCC, reverse, TCTTTGCCATGCATCTTGAC; *dHand* (57); *meis2*, forward, GTCCAATGGGAATGGGTATG, reverse, TGAGGCAACATAACGGAGTG; *Tbx5*, forward, CAGACTGGCCTTCAGTCTCC, reverse, CAACACTCAGCGAGCAATA; *Sox9* (58); and *Col2a1* (59). *In situ* hybridization was performed as described previously (60). Whole-mount *in situ* hybridization was performed as previously described (52). 3D reconstruction was performed from serial sections hybridized to *Col2a1* probes using Amira software (Amira 3.0; Mercury Computer Systems TGS).

Luciferase reporter assays. A conserved region 3,300 bases upstream from transcription start site of murine *Raldh2* comprising approximately 1,350 bp was amplified with specific primers GATCGCTAGCAGCCGAAGATCATCTTTC (forward) and GATCAGATCTTGTGTAGACCCCCAGGA (reverse) from genomic mouse DNA and cloned into pGL2-Enhancer (Promega; catalog E1621). This vector contains its own transcription start site for luciferase. Cos7 cells were cultured in 24-well plates and transfected with ExGen500 (Fermentas) with 150 ng promoter construct, 300 ng of required *Hoxd13* construct, and 15 ng renilla luciferase. Reporter assays were performed 24 hours after transfection with Dual-Glo Luciferase Assay System (Promega; catalog TM058) according to the manufacturer's instructions.

ChMM culture. ChMM cultures were prepared as described previously (61). For RA treatment, cells were grown in DMEM: F12 with 10% FCS, 0.2% chicken serum, 2 mM L-glutamine, and penicillin/streptomycin. Medium was replaced every day. RA (Sigma-Aldrich; catalog R2625) was dissolved in EtOH, disulfiram (Fluka; catalog 86720) in DMSO, and citral (Sigma-Aldrich; catalog C83007) in medium. Controls were treated either with EtOH or DMSO alone. Alcian blue staining of chMM cultures was



performed in 1% Alcian blue in 1 N HCl after fixation in Kahles fixative (28.9% vol/vol EtOH; 0.37% formaldehyde; 3.9% vol/vol acetic acid). Histomorphometric quantification was performed with AxioVision Outmess Software (Zeiss). For Hoxd13 analysis, cells were infected with concentrated viral supernatants containing the cDNA encoding WT Hoxd13, Hoxd13^{*7Ala}, and Hoxd13^{*14Ala}. Infection with empty RCAS virus (62) was used as a control. Culture medium (DMEM-F12, 2% chicken serum, 4 mM L-glutamine, and penicillin/streptomycin) was replaced every 2 days. For each condition, 4 replicates were performed in parallel. Real-time PCR was performed as previously described (63) with gene-specific primers. Quantification of incorporated Alcian blue was performed after extraction of the dye with 6M guanidium chloride by OD₅₉₅.

Primary mesenchymal cell culture. Murine primary mesenchymal cells were isolated at E13.5, when mutants can clearly be distinguished from normal littermates. Hand and food plates were collected and prepared as described above for chMM. Cells were grown in DMEM: F12 with 10% FCS, 1% penicillin/streptomycin, and L-glutamine. Medium was replaced every second day. Alcian blue staining of primary mesenchymal cultures was performed (see above), and quantification was done using AxioVision Outmess Software (Zeiss).

ChIP. ChMM cultures were infected with RCAS-BP virus expressing an N-terminal FLAG-tagged Hoxd13 and cultured for 5 days as previously described (64). For IP, chMM cultures were digested with 0.02% collagenase type IA, 0.02% trypsin, and 1% FCS in PBS for 30 minutes at 37°C. Approximately 10⁸ cells were pooled and washed once in PBS. Chromatin crosslinking and IP were performed as previously described (65) with an affinity-purified monoclonal anti-FLAG M2 antibody (Sigma-Aldrich; catalog F1804). Sonification conditions were 32 pulses with 30% output and 45 seconds between pulses on a Branson sonifier 450D using a 5-mm tip. Following IP and washing steps, crosslinks were reversed for 15 minutes at 98°C. DNA was digested for 30 minutes at 37°C with RNase A and subsequently with proteinase K for 20 minutes at 45°C, followed by purification with PCR purification (QIAquick; Qiagen) columns. Analysis was performed by real-time PCR using POWER SYBR Green PCR Master Mix (Applied Biosystems) and ABI 7900 HT real-time PCR Cyclor (Applied Biosystems), as described before (63), with gene specific primers. Primers were as follows: 1 forward, AATTTAAACTTGCAACTAGATCACACAT; 1 reverse, CCAGGTCACATTTATCATCTACTAAATG; 2 forward, GAGTGCTGTGTGCAAGGTGG; 2 reverse, CCCATCCAGTCTCACAGGTTC; 3 forward, AACACAGTGTAAATTTTTGAACTGA; 3 reverse, TCAGTGTTT-

GGGTATTTTAGAAGTCA; 4 forward, AAATCTGCGGTCTCTCCATT; 4 reverse, TCACCACGTGCACCTCTGTAA.

Bead implantation. Chicken eggs were incubated for 5 days. Beads (BioRad; catalog AGI-X2) were soaked with either 4 mg/ml RA (Sigma-Aldrich; catalog R2625) in DMSO, with 0.1 g/ml citral (Sigma-Aldrich; catalog C83007) in DMSO, or in DMSO alone. Beads were incubated at room temperature for 15 minutes and then directly used. Implanted chicken embryos were removed after 24 hours, fixed in 4% PFA overnight, and then prepared for paraffin embedding and section in situ hybridization as described above. A specific chicken ColII probe was used, as unimplanted limbs served as controls.

Immunohistochemistry. Immunohistochemistry was performed on 5-μm paraffin sections at E12.5 and E13.5. Sections were rehydrated in a descending series of EtOH concentrations, boiled in citrate buffer twice for 3 minutes, permeabilized with 0.2% Triton X-100 for 15 minutes, and blocked with normal goat serum. Antibody incubation was done at 4°C overnight with anti-Sox9 (1:50; Santa Cruz Biotechnology Inc.; catalog 20095) and for 1 hour with Alexa Fluor 488-conjugated secondary antibody (Invitrogen). Sample examination was done with an AxioVert 200 fluorescence microscope and AxioVision software (both Zeiss).

Statistics. For statistical analysis, the 2-tailed Student's *t* test was used. *P* values less than 0.05 were considered significant.

Acknowledgments

This work was supported by a grant from the Deutsche Forschungsgemeinschaft to S. Mundlos. We thank D. Duboule (University of Geneva, Geneva, Switzerland) for supplying us with Hoxd13^{*/+} mutant mice. We thank N. Rösener for help with genotyping, J. Wetzel for work with the mice, and O. Hagens for cloning chHoxd11 and chHoxd12 constructs. We also thank the Ressourcenzentrum für Genomforschung for chip hybridization and S. Reijntjes for teaching us implanting techniques.

Received for publication July 21, 2008, and accepted in revised form October 22, 2008.

Address correspondence to: Stefan Mundlos, Institut für Medizinische Genetik, Charité, Universitätsmedizin Berlin, Augustenburger Platz 1, 13353 Berlin, Germany. Phone: 49-30-450-569-121; Fax: 49-30-450-569-915; E-mail: stefan.mundlos@charite.de.

- Kornak, U., and Mundlos, S. 2003. Genetic disorders of the skeleton: a developmental approach. *Am. J. Hum. Genet.* **73**:447–474.
- Schwabe, G.C., and Mundlos, S. 2004. Genetics of congenital hand anomalies. *Handchir. Mikrochir. Plast. Chir.* **36**:85–97.
- Hill, R.E. 2007. How to make a zone of polarizing activity: insights into limb development via the abnormality preaxial polydactyly. *Dev. Growth Differ.* **49**:439–448.
- Robert, B., and Lallemand, Y. 2006. Anteroposterior patterning in the limb and digit specification: contribution of mouse genetics. *Dev. Dyn.* **235**:2337–2352.
- Tickle, C. 2006. Making digit patterns in the vertebrate limb. *Nat. Rev. Mol. Cell Biol.* **7**:45–53.
- Masuya, H., Sagai, T., Wakana, S., Moriwaki, K., and Shiroishi, T. 1995. A duplicated zone of polarizing activity in polydactylous mouse mutants. *Genes Dev.* **9**:1645–1653.
- Lettice, L.A., et al. 2002. Disruption of a long-range cis-acting regulator for Shh causes preaxial polydactyly. *Proc. Natl. Acad. Sci. U. S. A.* **99**:7548–7553.
- Klopocki, E., et al. 2008. A microduplication of the long range SHH limb regulator (ZRS) is associated with triphalangeal thumb-polysyndactyly syndrome. *J. Med. Genet.* **45**:370–375.
- Maas, S.A., and Fallon, J.F. 2005. Single base pair change in the long-range Sonic hedgehog limb-specific enhancer is a genetic basis for preaxial polydactyly. *Dev. Dyn.* **232**:345–348.
- Hill, P., Wang, B., and Rütger, U. 2007. The molecular basis of Pallister Hall associated polydactyly. *Hum. Mol. Genet.* **16**:2089–2096.
- Marshall, W.F., and Nonaka, S. 2006. Cilia: tuning in to the cell's antenna. *Curr. Biol.* **16**:R604–R614.
- Haycraft, C.J., et al. 2005. Gli2 and Gli3 localize to cilia and require the intraflagellar transport protein polaris for processing and function. *PLoS Genet.* **1**:e53.
- Chan, D.C., Laufer, E., Tabin, C., and Leder, P. 1995. Polydactylous limbs in Strong's Luxoid mice result from ectopic polarizing activity. *Development.* **121**:1971–1978.
- Babbs, C., Furniss, D., Morriss-Kay, G.M., and Wilkie, A.O.M. 2008. Polydactyly in the mouse mutant Doublefoot involves altered Gli3 processing and is caused by a large deletion in cis to Indian hedgehog. *Mech. Dev.* **125**:517–526.
- Malik, S., and Grzeschik, K. 2008. Synpolydactyly: clinical and molecular advances. *Clin. Genet.* **73**:113–120.
- Zakany, J., and Duboule, D. 2007. The role of Hox genes during vertebrate limb development. *Curr. Opin. Genet. Dev.* **17**:359–366.
- Fromental-Ramain, C., et al. 1996. Hoxa-13 and Hoxd-13 play a crucial role in the patterning of the limb autopod. *Development.* **122**:2997–3011.
- Davis, A.P., Witte, D.P., Hsieh-Li, H.M., Potter, S.S., and Capecchi, M.R. 1995. Absence of radius and ulna in mice lacking hoxa-11 and hoxd-11. *Nature.* **375**:791–795.
- Wellik, D.M., and Capecchi, M.R. 2003. Hox10 and Hox11 genes are required to globally pattern the mammalian skeleton. *Science.* **301**:363–367.
- Boulet, A.M., and Capecchi, M.R. 2004. Multiple roles of Hoxa11 and Hoxd11 in the formation of the mammalian forelimb zeugopod. *Development.* **131**:299–309.
- Muragaki, Y., Mundlos, S., Upton, J., and Olsen, B.R. 1996. Altered growth and branching patterns in synpolydactyly caused by mutations in HOXD13. *Science.* **272**:548–551.
- Goodman, F.R., et al. 1997. Synpolydactyly phenotypes correlate with size of expansions in HOXD13



- polyalanine tract. *Proc. Natl. Acad. Sci. U. S. A.* **94**:7458–7463.
23. Johnson, K.R., et al. 1998. A new spontaneous mouse mutation of Hoxd13 with a polyalanine expansion and phenotype similar to human synpolydactyly. *Hum. Mol. Genet.* **7**:1033–1038.
24. Albrecht, A., and Mundlos, S. 2005. The other trinucleotide repeat: polyalanine expansion disorders. *Curr. Opin. Genet. Dev.* **15**:285–293.
25. Bruneau, S., Johnson, K.R., Yamamoto, M., Kuroiwa, A., and Duboule, D. 2001. The mouse Hoxd13(spdh) mutation, a polyalanine expansion similar to human type II synpolydactyly (SPD), disrupts the function but not the expression of other Hoxd genes. *Dev. Biol.* **237**:345–353.
26. Albrecht, A.N., et al. 2004. A molecular pathogenesis for transcription factor associated poly-alanine tract expansions. *Hum. Mol. Genet.* **13**:2351–2359.
27. Dollé, P., et al. 1993. Disruption of the Hoxd-13 gene induces localized heterochrony leading to mice with neotenic limbs. *Cell.* **75**:431–441.
28. Zákány, J., Kmita, M., and Duboule, D. 2004. A dual role for Hox genes in limb anterior-posterior asymmetry. *Science.* **304**:1669–1672.
29. Zhao, D., et al. 1996. Molecular identification of a major retinoic-acid-synthesizing enzyme, a retinaldehyde-specific dehydrogenase. *Eur. J. Biochem.* **240**:15–22.
30. Wang, T., Zhang, H., and Parent, J.M. 2005. Retinoic acid regulates postnatal neurogenesis in the murine subventricular zone-olfactory bulb pathway. *Development.* **132**:2721–2732.
31. Tanaka, M., Tamura, K., and Ide, H. 1996. Citral, an inhibitor of retinoic acid synthesis, modifies chick limb development. *Dev. Biol.* **175**:239–247.
32. Bi, W., Deng, J.M., Zhang, Z., Behringer, R.R., and de Crombrughe, B. 1999. Sox9 is required for cartilage formation. *Nat. Genet.* **22**:85–89.
33. Ng, L.J., et al. 1997. SOX9 binds DNA, activates transcription, and coexpresses with type II collagen during chondrogenesis in the mouse. *Dev. Biol.* **183**:108–121.
34. Maden, M. 1982. Vitamin A and pattern formation in the regenerating limb. *Nature.* **295**:672–675.
35. Tickle, C., Alberts, B., Wolpert, L., and Lee, J. 1982. Local application of retinoic acid to the limb bud mimics the action of the polarizing region. *Nature.* **296**:564–566.
36. Mic, F.A., Sirbu, I.O., and Duester, G. 2004. Retinoic acid synthesis controlled by Raldh2 is required early for limb bud initiation and then later as a proximodistal signal during apical ectodermal ridge formation. *J. Biol. Chem.* **279**:26698–26706.
37. Niederreither, K., Vermot, J., Schuhbauer, B., Chambon, P., and Dollé, P. 2002. Embryonic retinoic acid synthesis is required for forelimb growth and antero-posterior patterning in the mouse. *Development.* **129**:3563–3574.
38. Lu, H.C., Revelli, J.P., Goering, L., Thaller, C., and Eichele, G. 1997. Retinoid signaling is required for the establishment of a ZPA and for the expression of Hoxb-8, a mediator of ZPA formation. *Development.* **124**:1643–1651.
39. de Thé, H., Vivanco-Ruiz, M.M., Tiollais, P., Stunnenberg, H., and Dejean, A. 1990. Identification of a retinoic acid responsive element in the retinoic acid receptor beta gene. *Nature.* **343**:177–180.
40. Allenby, G., et al. 1993. Retinoic acid receptors and retinoid X receptors: interactions with endogenous retinoic acids. *Proc. Natl. Acad. Sci. U. S. A.* **90**:30–34.
41. Mercader, N., et al. 2000. Opposing RA and FGF signals control proximodistal vertebrate limb development through regulation of Meis genes. *Development.* **127**:3961–3970.
42. Weston, A.D., Hoffman, L.M., and Underhill, T.M. 2003. Revisiting the role of retinoid signaling in skeletal development. *Birth Defects Res. C Embryo Today.* **69**:156–173.
43. Zimmermann, B., and Tsambaos, D. 1985. Evaluation of the sensitive step of inhibition of chondrogenesis by retinoids in limb mesenchymal cells in vitro. *Cell Differ.* **17**:95–103.
44. Wedden, S.E., Lewin-Smith, M.R., and Tickle, C. 1987. The effects of retinoids on cartilage differentiation in micromass cultures of chick facial primordia and the relationship to a specific facial defect. *Dev. Biol.* **122**:78–89.
45. Desbiens, X., Meunier, L., and Lassalle, B. 1990. Specific effects of retinoic acid on the skeletal morphogenesis of the 11-day mouse embryo forelimb bud in vitro. *Biol. Cell.* **68**:213–220.
46. Hoffman, L.M., et al. 2006. BMP action in skeletogenesis involves attenuation of retinoid signaling. *J. Cell Biol.* **174**:101–113.
47. Weston, A.D., Rosen, V., Chandraratna, R.A., and Underhill, T.M. 2000. Regulation of skeletal progenitor differentiation by the BMP and retinoid signaling pathways. *J. Cell Biol.* **148**:679–690.
48. Weston, A.D., Chandraratna, R.A.S., Torchia, J., and Underhill, T.M. 2002. Requirement for RAR-mediated gene repression in skeletal progenitor differentiation. *J. Cell Biol.* **158**:39–51.
49. Serpente, P., et al. 2005. Direct crossregulation between retinoic acid receptor {beta} and Hox genes during hindbrain segmentation. *Development.* **132**:503–513.
50. Simeone, A., et al. 1990. Sequential activation of HOX2 homeobox genes by retinoic acid in human embryonal carcinoma cells. *Nature.* **346**:763–766.
51. Zákány, J., Fromental-Ramain, C., Warot, X., and Duboule, D. 1997. Regulation of number and size of digits by posterior Hox genes: a dose-dependent mechanism with potential evolutionary implications. *Proc. Natl. Acad. Sci. U. S. A.* **94**:13695–13700.
52. Albrecht, A.N., et al. 2002. The synpolydactyly homolog (spdh) mutation in the mouse – a defect in patterning and growth of limb cartilage elements. *Mech. Dev.* **112**:53–67.
53. Zákány, J., and Duboule, D. 1996. Synpolydactyly in mice with a targeted deficiency in the HoxD complex. *Nature.* **384**:69–71.
54. Lohnes, D., et al. 1994. Function of the retinoic acid receptors (RARs) during development (I). Craniofacial and skeletal abnormalities in RAR double mutants. *Development.* **120**:2723–2748.
55. Hurler, J.M., and Gañan, Y. 1987. Formation of extra-digits induced by surgical removal of the apical ectodermal ridge of the chick embryo leg bud in the stages previous to the onset of interdigital cell death. *Anat. Embryol. (Berl.)* **176**:393–399.
56. Klose, J., and Kobalz, U. 1995. Two-dimensional electrophoresis of proteins: an updated protocol and implications for a functional analysis of the genome. *Electrophoresis.* **16**:1034–1059.
57. Niedermaier, M., et al. 2005. An inversion involving the mouse Shh locus results in brachydactyly through dysregulation of Shh expression. *J. Clin. Invest.* **115**:900–909.
58. Healy, C., Uwanogho, D., and Sharpe, P.T. 1999. Regulation and role of Sox9 in cartilage formation. *Dev. Dyn.* **215**:69–78.
59. Kohno, K., Martin, G.R., and Yamada, Y. 1984. Isolation and characterization of a cDNA clone for the amino-terminal portion of the pro-alpha 1(II) chain of cartilage collagen. *J. Biol. Chem.* **259**:13668–13673.
60. Stricker, S., Fundele, R., Vortkamp, A., and Mundlos, S. 2002. Role of Runx genes in chondrocyte differentiation. *Dev. Biol.* **245**:95–108.
61. Seemann, P., et al. 2005. Activating and deactivating mutations in the receptor interaction site of GDF5 cause symphalangism or brachydactyly type A2. *J. Clin. Invest.* **115**:2373–2381.
62. Federspiel, M.J., and Hughes, S.H. 1997. Retroviral gene delivery. *Methods Cell Biol.* **52**:179–214.
63. Hecht, J., et al. 2007. Detection of novel skeletogenesis target genes by comprehensive analysis of a Runx2(-/-) mouse model. *Gene Expr. Patterns.* **7**:102–112.
64. Lehmann, K., et al. 2003. Mutations in bone morphogenetic protein receptor 1B cause brachydactyly type A2. *Proc. Natl. Acad. Sci. U. S. A.* **100**:12277–12282.
65. Lee, T.I., Johnstone, S.E., and Young, R.A. 2006. Chromatin immunoprecipitation and microarray-based analysis of protein location. *Nat. Protoc.* **1**:729–748.